Intrinsic properties of osteomalacia bone evaluated by nanoindentation and FTIRM analysis

Insaf Hadjab, Delphine Farlay, Pierrick Crozier, Thierry Douillard, Georges Boivin, Jérome Chevalier, Sylvain Meille, Hélène Follet

Intrinsic Properties of Osteomalacia Bone evaluated by Nanoindentation and FTIRM Analysis

I. Hadjab[1, 2], D. Farlay[1], P. Crozier[3], T. Douillard[3], G. Boivin[1], J. Chevalier[3], S. Meille[3], H. Follet[1]

1 : Univ Lyon, Université Claude Bernard Lyon 1, INSERM, LYOS UMR1033, F69008, Lyon, France
2 : Now, in École Polytechnique de Montréal, Canada
3 : Univ Lyon, INSA-LYON, MATEIS, UMR CNRS 5510, F69621, Villeurbanne, France ;
Corresponding author: H. Follet, helene.follet@inserm.fr

Insaf Hadjab : hadjab.insaf@gmail.com
École Polytechnique de Montréal, Canada.
Delphine Farlay : delphine.farlay@inserm.fr
INSERM, UMR1033 ; Université De Lyon, FRANCE
Pierrick Crozier: pierrickcrozier@gmail.com
Centre Hospitalier Universitaire de Nice, France
Thierry Douillard : Thierry.Douillard@insa-lyon.fr
CNRS, UMR5510, Université De Lyon, France
Georges Boivin : georges.boivin@univ-lyon1.fr
INSERM, UMR1033 ; Université De Lyon, FRANCE
Jérôme Chevalier : jerome.chevalier@insa-lyon.fr
CNRS, UMR5510, Université De Lyon1, France,
Sylvain Meille : Sylvain.Meille@insa-lyon.fr
CNRS, UMR5510, Université De Lyon, France
Helene Follet : helene.follet@inserm.fr
INSERM, UMR1033 ; Université De Lyon, FRANCE

Word count : 3607

Abstract

Osteomalacia is a pathological bone condition consisting in a deficient primary mineralization of the matrix, leading to an accumulation of osteoid tissue and reduced bone mechanical strength. The amounts, properties and organization of bone constituents at tissue level, are known to influence its mechanical properties. It is then important to investigate the relationship between mechanical behavior and tissue composition at this scale in order to provide a better understanding of bone fragility mechanisms associates with this pathology.

Our purpose was to analyze the links between ultra-structural properties and the mechanical behavior of this pathological bone tissue (osteomalacia) at tissue level (mineral and osteoid separately, or global). Four bone biopsies were taken from patients with osteomalacia, and subsequently embedded, sectioned, and polished. Then nanoindentation tests were performed to determine local elastic modulus E, contact hardness Hc and true hardness H for both mineralized and organic bone phases and for the global bone. The creep of the bone was also studied using a special indentation procedure in order to assess visco-elasto-plastic (creep) bone behavior. This allowed a detailed study of the rheological models adapted to the bone and to calculate the parameters associated to a Burgers model. Ultra-structural parameters were measured by Fourier Transform InfraRed Microspectroscopy (FTIRM) on the same position as the indents.

The use of rheological models confirmed a significant contribution from the organic phase on the viscous character of bone tissue. The elastic E and the elasto-plastic H_c deformation were correlated to both collagen maturity and Mineral/Matrix. The pure plastic deformation H was only correlated to the mineral phase. Our data show that mineral phase greatly affects mechanical variables (moduli and viscosities) and that organic phase (as illustrated in osteoid tissue) may play an important role in the creep behavior of bone. In conclusion, this study brings mechanical and physicochemical values for osteoid and mineral phases.

Keywords: Human bone tissue, osteomalacia, nanoindentation, FTIRM.

I- Introduction

Bone is a multiscale architectured composite with a heterogeneous and hierarchical structure, consisting of mineral deposits composed of crystalline apatite on an organic matrix, presented mainly by type I collagen network (Bala et al., 2011; Burr, 2002; Oyen, 2019; Rho et al., 1998). The remodeling process contributes to calcium and phosphorous homeostasis and leads to the formation of Bone Structural Units (BSUs) (Hadjidakis and Androulakis, n.d.). The formation starts first with the synthesis of the organic matrix (osteoid) followed by mineralization of apatite crystals (Bala et al., 2010; Boivin and Meunier, 2003, 2002).

Osteomalacia is a bone pathology associated to a deficient primary mineralization of the matrix, leading to an accumulation of osteoid tissue and reduced bone mechanical strength (Faibish et al., 2005).

The mineral content in bone influences its stiffness and strength (Bala et al., 2011; Boivin et al., 2008; Follet et al., 2004), while the mechanical function of organic matrix remains barely understood (Currey, 2003). Patients affected by this osteomalacia suffer from a decreased mineralized bone leading to an increase in the organic matrix content, through the increase of the osteoid thickness (Bhan et al., 2018; Bonucci et al., 1969; Faibish et al., 2005; Turner et al., 1996). Collagen content and chemistry may also play a role in determining viscoelastic behavior of bone (Donnelly et al., 2006; Wu et al., 2012). This enables to consider this tissue as a good model to access directly to the organic matrix study (Oyen, 2008; Rho et al., 1999).

For a better understanding of the biomechanical properties of healthy and diseased bones, several studies have been done to establish their relationships with the composition at a local scale (Bala et al., 2011, 2010; Cai et al., 2019; Farlay et al., 2010; Lefèvre et al., 2019).

Indentation techniques have been widely used over the past two decades to study a large range of viscoelastic materials including biological tissues and in particular bone viscoelasticity (Bembey et al., 2006; Fan and Rho, 2003; Oyen, 2005; Oyen and Cook, 2003; Rho and Pharr, 1999; Tang et al., 2007). Nano-indentation technique with a Berkovich tip can be used to investigate the tissue-level mechanical properties and site-specific variations within different individual structures (lamellae/osteons) and for different types of tissues (osteoid vs mineralized) (Bala et al., 2011; Farlay et al., 2019; Rho and Pharr, 1999; Zysset et al., 1999). Indentation tests are often analyzed assuming an elasto-plastic behaviour of the bone, with

time-independent elastic and plastic parameters, such as the Young's modulus E, contact hardness H_c and true hardness H as determined by (Sakai, 1999).

Since bone possesses inherently time-dependent behaviour, the viscous response should also be taken in consideration when analysing indentation tests (Bembey et al., 2006; Oyen and Ko, 2007). Specific testing procedures are used to characterize the viscoelastic properties of mineralized tissues, for example by applying a constant load and subsequently measuring the creep depth as a function of time. Several analytical approaches have been developed, mostly based on a combination of viscoelastic constitutive laws to account for load-time responses of bone and enamel (He and Swain, 2009; Oyen, 2005; Oyen and Ko, 2007). A Visco-Elasto-Plastic (VEP) creep model for time-dependent indentation (Oyen, 2006) has been investigated in terms of experimentally-derived variables of load, displacement, and time (Oyen and Cook, 2003). Isaksson et al. have chosen a Burgers model to simulate the VEP creep response of bone, since it enables to capture the immediate elastic response during indentation (Isaksson et al., 2010b).

Fourier Transform InfraRed Microspectroscopy (FTIRM) presents a powerful micro-spectroscopic technique which allows the collection of detailed information about bone composition, mineral and organic properties (such as Mineral/Matrix and collagen maturity respectively), which are important for the viscous micromechanical properties (Bala et al., 2011, 2010; Bonucci et al., 1969; Boskey, 2003; Boskey and Imbert, 2017; Carden and Morris, 2000; Farlay et al., 2010; Farlay and Boivin, 2012).

Histologic analysis have been done (Bhan et al., 2018, 2010), but only few mechanical studies have been conducted on osteomalacia bone (Boivin et al., 2008).

Our hypothesis is that specific links exist between micro-structural properties and mechanical behavior of osteomalacia bone tissue. The purpose of this study was thus to characterize the variation in viscous, elastic and plastic properties of bone organic matrix at tissue level (mineral and osteoid separately, or global). Micromechanical parameters were assessed by indentation probing, dynamic (Continuous Stiffness Mode, CSM) and quasi-static (creep) testing protocols. These data were analyzed with Burger rheological model to quantify the time-dependent visco-elasto-plastic mechanical properties. Furthermore, we evaluated the relationships between these data with measured Mineral/Matrix and collagen maturity.

II -Material and Methods

2.1. Sample preparation

Four transiliac bone samples taken from 50±11 year-old patients (2 males, 2 females) with osteomalacia (one after gastrectomy, one renal osteodystrophy, two unknowns) were used (approval from Hospital Ethics Committee as an usual care study). Confirmation of the diagnosis of osteomalacia was defined on bone biopsies as a strong increase in osteoid thickness with a decrease in the mineral apposition rate. The methods used for the preparation of samples was described previously (Bala et al., 2011; Boivin et al., 2008). Briefly, undecalcified samples were fixed in 70% alcohol, dehydrated in absolute alcohol, and then embedded in poly-methyl methacrylate (PMMA). For instrumented nano-indentation, 150 µm-thick sections were cut in a perpendicular plan to the Haversian canals with a precision diamond wire saw (Well, Escil, Chassieu, France), then ground progressively (silicium carbides) to a thickness of 100±1µm and polished with a diamond suspension (0.25µm) (Boivin and Meunier, 2002). These sections were indented and then re-sectioned into 2µm-thick sections to perform FTIRM (Polycut E microtome, Leica, Germany), (Figure 1).

2.2. Nanoindentation testing

Nano-indentation tests were carried out using a Nano Indenter II machine (Nano Instruments Inc., USA) equipped with a Berkovich diamond tip. The system was calibrated with fused silica according to (Oliver and Pharr, 1992)'s protocol. Bone Structural Units (BSUs) were selected on each bone biopsy, resulting in total amount of 303. Those BSUs selected were indented. The indent location was chosen at sites distant from visible lacunae or other discontinuities. Tests were also performed in the impregnation resin PMMA next to the sample, in order to characterize its properties and its possible influence on the measurement of bone tissue. Two different procedures were used: a continuous stiffness mode (CSM) test to estimate elastic and plastic parameters and a creep test to characterize the viscous parameters of the tissue at the BSU level. In CSM, 260 indents were done on four samples, with 115 in osteoid tissue and 145 in mineralized tissue, both in cortical and cancellous bone. For Creep tests, 43 indents were analyzed on three samples, 19 in osteoid tissue and 24 in mineralized tissue.

The CSM test followed the methods used in (Bala et al., 2011) to measure elastic modulus and hardness versus the displacement of the indenter. This procedure consisted in a displacement-controlled loading phase until a total penetration depth of 5120 nm. This value

enabled to characterize the tissue at the BSU scale, averaging the heterogeneity of the structure at the lamellar scale and limiting the influence of samples roughness on the measurements. A 0.05 s^{-1} constant strain rate loading stage was followed by a 10 s dwell at the maximum load, and by a 45 s withdrawal to 10% of maximum displacement, a 50 s hold period for thermal drift calculation and final withdrawal to zero displacement. The testing procedure is synthetized in Figure 2.

The Young's modulus (E) and the contact hardness ($H_{c)}$ were determined following Oliver & Pharr method for the estimation of the contact area (Oliver and Pharr, 1992), using a custom Matlab code (Math Works Inc., Natik MA, USA) to process the individual load displacement curves as detailed in (Bala et al., 2011). For each indent, true hardness (H), which reflects only the plastic character of the material was calculated based on the previous parameters (E) and (H_c) (Sakai, 1999). The true hardness (H) was then deduced as described previously by (Bala et al., 2011). The total, elastic, and plastic works were also computed from the load-displacement curves, and, for analyses, only the ratio W_{plast}/W_{tot} was used since it represents surrogate measurements of irreversible mechanisms occurring during indentation (Mirzaali et al., 2016).

The creep experiments were conducted at a constant load of 150 mN for 240 s (4 min) to measure changes in the indentation depth versus time (Figure 2). Both loading and unloading were performed at a constant loading speed of 15mN.s^{-1}. The penetration depth after loafing was typically of 3.5 µm and 5 µm for mineralized and osteoid tissues respectively, to avoid the influence of surface roughness after polishing as well as to overcome the influence of heterogeneity at the lamellar scale. The penetration depth during the dwell at constant load was recorded and was further post-processed to characterize the non-linear characteristics of the tissues, as well as the one of the PMMA as a benchmark and further analysis.

The analysis procedure was performed following (Vandamme and Ulm, 2006) approach on both loading and holding segments curves. Burgers model (see Figure 2C) implies four parameters: two elastic modulus E_1, E_2 and two viscosities η_1, $\eta_{2;}$ parameters reflecting the local VEP behavior for each indent (Figure 2). The signification of different parameters should be understood as follows: E_1 (in GPa) governs the "instantaneous" elastic behavior of the material, η_1 (in GPa.s) characterize the permanent deformation, i.e. the plastic properties, and E_2 (in GPa) and η_2 (in GPa.s) the viscoelastic properties. L is the total length of creep during the load hold segment (µm).

The calculation of the parameters was done by fitting experimental curves with the rheological equations of Burgers model (Fig 2C) for conical indentation as derived by (Vandamme and Ulm, 2006), using a Levenberg-Marquardt algorithm with a custom Matlab code. The partial derivatives needed for the analysis procedure have been calculated using Maple (Maplesoft, Waterloo, Canada) for verification purposes. The Berkovich tip used for experiments was considered as modeled by an equivalent conical indenter of apex 70.3°. The Poisson's ratio for all tests is set to 0.3, and the hypothesis of an isotropic behavior is considered.

2.3. Fourier Transform InfraRed Microspectroscopy (FTIRM)

Due to the process (re-cut section of 2µm from the previous one), only three samples were available. FTIRM was performed on 30×55 μm^2 area with 30 positions per sample, which were tested previously with nanoindentation. The spectra were collected in transmission mode with a Spectrum 100 spectrometer equipped with an Auto-IMAGE microscope (Perkin-Elmer, Shelton, Connecticut, USA). Each spectrum corresponded to 100 cumulated scans. The contributions of air and PMMA were subtracted from the individual spectra, and a baseline at absorbance 2 was corrected and normalized on the ν_3PO_4. Following the same procedure used by (Bala et al., 2011), the spectra were curve-fitted using GRAMS/AI software (Thermo galactic, Salem, New Hampshire, USA) to analyze the peaks ν_4 PO_4 (500–650 cm^{-1}) and amides I (1600–1700 cm^{-1}). A total amount of 160 spectra were analyzed.

The mineral to organic ratio (Mineral/Matrix) was measured as the areas ratio at the peak of 1030 cm^{-1} ($\nu_1\nu_3PO_4$) and the peak of 1660 cm^{-1} which is the main peak of amides I. Collagen maturity (Col Mat) was evaluated by the ratio of the peaks area (1660 cm^{-1} /1690 cm^{-1}) (Farlay et al., 2011; Paschalis et al., 2001). Crystallinity index was calculated as the inverse of the full width at half max of the 604 cm^{-1} peak (Farlay et al., 2010).

2.4. Statistical analysis

Statistical analysis was performed under SPSS v16.0 (SPSS inc., Chicago Illinois, USA) using an alpha risk set at 5%. Results were reported as mean± standard deviation (SD). The distribution of the variables was tested with Kruskal-Wallis & Mann-Whitney nonparametric procedure. The influence of the microstructure on the micromechanical

159 behavior was studied using linear regression analyses (ρ: Spearman's Rho correlation
160 coefficient).

161 For the paired comparison, only indents which have undergone both mechanical and
162 physicochemical characterizations were used (Figure 1, Physicochemical parameters and
163 CSM: 116; and creep: 43).

III- Results

Significant differences were observed in both mechanical ($p<0.0001$) and physicochemical parameters ($p<0.05$) according to bone tissue-type (osteoid / mineralized), (Table 1). We chose to present results for the global tissue, and for the mineral and osteoid part.

Physicochemical parameters (Table 1, Figure 3 A, Table 2)

The Mineral/Matrix was significantly lower in the osteoid tissue than in the mineralized one (resp. 0.20±0.18, 3.62±1.28, $p<0.0001$). Identically, collagen maturity (Col Mat) varies from 3.39±1.34 in osteoid to 4.23±1.46, ($p<0.0001$) in mineralized tissue, whereas crystallinity was only available in mineralized tissue 0.04± 0.003 (Table 1). Col Mat and Mineral/Matrix were positively correlated in mineralized tissue ($\rho=0.560$; $p<0.001$), while they were weakly and negatively correlated in osteoid tissue ($\rho=-0.284$; $p<0.05$), (Figure 3A, Table 2). Mineral/Matrix is significantly correlated with crystallinity in the mineral compartment (0.316, $p<0.01$). Crystallinity is also linked to Col Mat (0.238, $p<0.05$).

Mechanical parameters (Table 1&2, Figure 3 B&C, Figure 4)

Figure 3b shows representative load - displacement curves for mineral, osteoid and PMMA resin. A large difference is noted in the maximum load for a similar penetration depth in each zone, revealing a higher hardness and stiffness of mineral tissue as compared to osteoid tissue and impregnation resin. Micromechanical CSM variables (E, $H_{c,}$ and H) reflecting the elastic, elasto-plastic and pure plastic response respectively were deduced from load-displacement curves. Their values decreased respectively from 12.2±2.7, 0.52±0.12 and 1.85±0.5GPa in mineralized tissue to 5.04±0.8, 0.22±0.05 and 0.81±0.3GPa in osteoid tissue. The ratio of irreversible work to the total work represented by W_{plast}/W_{tot} is also slightly higher in mineral (0.71±0.03) than in osteoid tissue (0.67±0.03) and is significantly correlated to H/E as already noted for structural materials (data not shown, (Cheng and Cheng, 1998)).

Linear regression revealed strong and positive correlations ($\rho=0.946$, $p<0.001$) between the elastic modulus (E) and the contact hardness (H_c), both in osteoid ($\rho=0.730$; $p<0.001$) and

in mineralized tissue ($\rho=0.848$; $p<0.001$) (Figure 3B, Table 2). The true hardness (H) reflecting the plastic behavior was also strongly correlated with E ($\rho=0.856$, $p<0.001$) for both

osteoid (ρ=0.451; p<0.001) and mineralized tissues (ρ=0.610; p<0.001). Except for H_c in the mineral compartment, W_{plast}/W_{tot} is significantly correlated with other mechanical parameters. Characteristic time - displacement curves in creep mode for mineral, osteoid tissues and for PMMA resin are shown in Figure 4. These curves revealed a strong difference between mechanical behavior between the different zones tested, with a larger creep displacement L for PMMA resin and for osteoid tissue as compared to mineralized tissue. PMMA exhibits the largest viscous component. The values of different Creep modulus E_1 and E_2 and viscosities η_1 and η_2 are larger in mineralized tissues (Table 1) than in osteoid tissue, by a factor ranging from 1.9 (for η_2) to 2.9 (for η_1). From a global interpretation, parameters are significantly and positively correlated (Table 2). However, the length of creep was negatively correlated with both elastic modulus of Burgers model.

Comparing the CSM and Creep modes using the mean within each compartment (mineral and osteoid), for the three separate samples, E and E_1, reflecting the similar elastic properties, are significantly correlated (ρ=0.943,p< 0.01). In a similar manner, plastic parameters are linked (H and η_1, ρ= 0.943;p<0.01).

Relationships between Physicochemical and Mechanical parameters (Table 2, Figure 5)

Mineral/Matrix was significantly correlated with all micromechanical parameters (E; H_c; H) in the global osteomalacia bone tissue (ρ=0.867; 0.831; 0.761 *resp.*, p<0.001). These correlations, even significant, were more moderate within the mineralized tissue (ρ=0.647; 0.558; 0.458 *resp.*,p<0.001). While in osteoid tissue, only the elastic modulus was significantly correlated with Mineral/Matrix (ρ=0.285,p<0.05) (Figure 4, Table 2). Similar results are observed for the creep mode (Table 2). Linear regression demonstrated a moderate positive correlation between collagen maturity and respectively E (ρ=0.272,p<0.01) and H_c (ρ= 0.220,p<0.05) for the global tissue. This relationship remains valuable only between the Col Mat and the elastic modulus E within the mineralized tissue (ρ=0.410,p< 0.01) and H_c (ρ=0.269,p<0.05), and no relationships has been found in osteoid tissue. Relationships are plotted in Figures 5. Crystallinity does not show relationship except with E.

For all bone samples, the parameters of Burgers model were significantly correlated with the Mineral/Matrix parameters (Table 2). All these correlations were positive, except for the creep length L. The viscosity η_1 presents the highest correlation coefficient with the Mineral/Matrix, (ρ= 0.828,p< 0.001). A similar relationship was observed with the collagen

maturity ($\rho = 0.554, p < 0.001$). Time-displacement creep curves were plotted for several indents within the same sample (Figure 4B). Each indent showed similar results with the same loading condition. More is the creep length, less is the collagen maturity.

IV-Discussion

The present study on human subjects with osteomalacia investigated the relationships between bone visco-elasto-plastic parameters and ultrastructural components, examined at the tissue level.

For the physicochemical parameters, values obtained in our study confirm what previous authors (Faibish et al., 2005; Farlay et al., 2019) found with low Mineral/Matrix ratio in osteomalacia. On the other side, we found a significant difference in Col Mat in osteoid and mineral phase. There is still a positive correlation between Col Mat and Mineral/Matrix, as in control bone, showing Col Mat is dependent of the quantity of deposed mineral. In the osteoid phase, there is a high heterogeneity of Col Mat, but values remain close to those obtained in the mineral phase. This suggests that if the organic matrix is relatively normal, the mineralization is however disturbed by calcium deficiency.

The micromechanical properties in both dynamic (CSM mode) and quasi-static (creep mode) and also those reflecting the ultrastructural variables (Mineral/Matrix, Col Mat) were consistent with previous studies. (Bala et al., 2011, 2010; Boivin et al., 2008; Farlay et al., 2010; Isaksson et al., 2010a; Lefèvre et al., 2019). In particular, the degree of mineralization is strongly correlated with the elastic modulus and hardness (Bala et al., 2011). This work also shows its correlation with the viscosity of mineralized tissue. It is usually claimed that elastic and plastic properties are related respectively to the mineral and collagen (Viguet-Carrin et al., 2006). A link was also recently found between collagen fibril scale and macroscale for elastic behavior in children's bone (Dépalle et al., 2018). But, to our knowledge, this study is the first to focus on the link between viscous response and ultrastructural variables.

In CSM mode, compared to (Bala et al., 2011), we found that both collagen maturity and in mineral tissue were 4.23 ±1.46 , and 0.040 ±0.003 respectively, compared to 4.69 ±0.76 and 0.040 ±0.002 in (Bala et al., 2011). Comparing with Vickers micro-hardness, (Boivin et al., 2008) concluded from their observations in human iliac bone that osteoid tissue represented about one third of the Hc of mineralized matrix, as in our study. As (Bala et al., 2011), we found that both collagen maturity and Mineral/Matrix play a role in elastic

deformation. Col Mat was also found correlated with the elasto-plastic H_c deformations, but not with the pure plastic H. But in this previous study, osteoporotic bones were used.

In creep mode, the osteoid tissue presents a larger value of creep length L than mineralized tissue, which reflects the primary role of organic phase in the viscous behavior of bone. For the entire tissue, L, was found also inversely correlated with the collagen maturity. Nano-indentation on demineralized tissue with acidic treatments, shows plastic deformations close to the tip of indenter correlated to a loss of the supramolecular bending structure in collagen fibrils (Tai et al., 2005). There is also evidence showing the role of collagen in the time-dependent deformation of bone under loading during indentation testing (Isaksson et al., 2010b).

We have shown that both collagen maturity & Mineral/Matrix were significantly correlated with most parameters of creep model, when considering the entire bone (both mineralized and osteoid tissues), confirming our hypothesis. There is also a trend to have a higher length L linked to collagen maturity in the osteoid tissue, but it is only significant when considering the global bone. Nevertheless, the major influence of Mineral/Matrix on the mechanical parameters of osteomalacia bone is clearly evidenced in this work.

Limitations: We investigated exclusively osteoid from diseased cases and for a quite small number of samples due to the difficulty in obtaining such specific cases. Moreover, the impregnation of bone samples by PMMA certainly has an influence on the mechanical properties of the tissues as compared to fresh samples. The qualitative comparison of properties between mineralized and osteoid tissues is however not influenced by the impregnation of PMMA resin, at the latter shows the lowest mechanical properties (Figures 3, 4 and 5). The impregnation of the porous phase by PMMA may explain the low correlation between mechanical parameters with structural parameters apart from the strong influence of mineral fraction confirmed in this study. The comparison of osteoid tissue with collagen is also certainly affected by the conservation protocol of the tested samples. The use of fresh sample seems however impossible, at least, using those technics. Following the study of (Diez-Perez et al., 2010), an *in vivo* measurement of parameters reflecting bone quality could be a possible option (Crespo, 2020).

In conclusion, this study brings mechanical and physicochemical values for osteoid and mineral phases. Only few studies were able to establish those relationships. However, our data show that mineral phase greatly affects mechanical variables (moduli and viscosities) and that

organic phase (as illustrated in osteoid tissue) may play an important role in the creep behavior of bone. The ratio osteoid/mineral in osteomalacia bone is such higher than in a control bone, that osteoid tissue influences the behavior of the entire bone, and lead to a more ductile bone. This could cause an increase of fractures risk as the remaining mineral has to sustain the entire daily activities load.

Conflict of interest statement

None of the authors have any conflicts of interest.

Ethics

The work was performed in compliance with ethical standards.

Acknowledgments

The authors gratefully acknowledge Jean-Paul Roux and Yohann Bala, Ph.D., for their helpful discussions and comments during the preparation of this study; and Anne-Sophie Bravo-Martin for her technical assistance.

References

Bala, Y., Depalle, B., Douillard, T., Meille, S., Clément, P., Follet, H., Chevalier, J., Boivin, G., 2011. Respective roles of organic and mineral components of human cortical bone matrix in micromechanical behavior: an instrumented indentation study. Journal of the mechanical behavior of biomedical materials 4, 1473–1482.

Bala, Y., Farlay, D., Delmas, P.D., Meunier, P.J., Boivin, G., 2010. Time sequence of secondary mineralization and microhardness in cortical and cancellous bone from ewes. Bone 46, 1204–1212. https://doi.org/10.1016/j.bone.2009.11.032

Bembey, A.K., Oyen, M.L., Bushby, A.J., Boyde, A., 2006. Viscoelastic properties of bone as a function of hydration state determined by nanoindentation. Philosophical Magazine 86, 5691–5703. https://doi.org/10.1080/14786430600660864

Bhan, A., Qiu, S., Rao, S.D., 2018. Bone histomorphometry in the evaluation of osteomalacia. Bone Reports 8, 125–134. https://doi.org/10.1016/j.bonr.2018.03.005

Bhan, A., Rao, A.D., Rao, S., 2010. Osteomalacia as a Result of Vitamin D Deficiency. Endocrinol. Metabol. Clin. North Amer. 39, 321-+. https://doi.org/10.1016/j.ecl.2010.02.001

Boivin, G., Bala, Y., Doublier, A., Farlay, D., Ste-Marie, L.G., Meunier, P.J., Delmas, P.D., 2008. The role of mineralization and organic matrix in the microhardness of bone tissue from controls and osteoporotic patients. Bone 43, 532–538. https://doi.org/10.1016/j.bone.2008.05.024

Boivin, G., Meunier, P.J., 2003. Methodological considerations in measurement of bone mineral content. Osteoporos Int 14 Suppl 5, S22-27; discussion S27-28. https://doi.org/10.1007/s00198-003-1469-1

Boivin, G., Meunier, P.J., 2002. The degree of mineralization of bone tissue measured by computerized quantitative contact microradiography. Calcified tissue international 70, 503–511.

Bonucci, E., Denys-Matrajt, H., Tun-Chot, S., Hioco, D., 1969. Bone Structure in Osteomalacia, with Special Reference to Ultrastructure. The Journal of Bone and Joint Surgery. British volume Vol. 51-B, No. 3, p 511–528.

Boskey, A., 2003. Bone mineral crystal size. Osteoporosis international 14, 16–21.

Boskey, A.L., Imbert, L., 2017. Bone quality changes associated with aging and disease: a review. Ann N Y Acad Sci 1410, 93–106. https://doi.org/10.1111/nyas.13572

Burr, D.B., 2002. The contribution of the organic matrix to bone's material properties. Bone 31, 8–11. https://doi.org/10.1016/S8756-3282(02)00815-3

Cai, X., Follet, H., Peralta, L., Gardegaront, M., Farlay, D., Gauthier, R., Yu, B., Gineyts, E., Olivier, C., Langer, M., Gourrier, A., Mitton, D., Peyrin, F., Grimal, Q., Laugier, P., 2019. Anisotropic elastic properties of human femoral cortical bone and relationships with composition and microstructure in elderly. Acta Biomaterialia 90, 254–266. https://doi.org/10.1016/j.actbio.2019.03.043

Carden, A., Morris, M.D., 2000. Application of vibrational spectroscopy to the study of mineralized tissues. Journal of biomedical optics 5, 259–269.

Cheng, Y.-T., Cheng, C.-M., 1998. Relationships between hardness, elastic modulus, and the work of indentation. Appl. Phys. Lett. 73, 614–616. https://doi.org/10.1063/1.121873

Crespo, D.O., 2020. Microindentation: A New Technique for Bone Quality Assessment. Adv. Ther. 37, 47–54. https://doi.org/10.1007/s12325-019-01175-2

Currey, J.D., 2003. Role of collagen and other organics in the mechanical properties of bone. Osteoporos Int 14 Suppl 5, S29-36. https://doi.org/10.1007/s00198-003-1470-8

Dépalle, B., Duarte, A.G., Fiedler, I.A., Pujo-Menjouet, L., Buehler, M.J., Berteau, J.-P., 2018. The different distribution of enzymatic collagen cross-links found in adult and children bone result in different mechanical behavior of collagen. Bone 110, 107–114.

Diez-Perez, A., Guerri, R., Nogues, X., Caceres, E., Jesus Pena, M., Mellibovsky, L., Randall, C., Bridges, D., Weaver, J.C., Proctor, A., Brimer, D., Koester, K.J., Ritchie, R.O., Hansma, P.K., 2010.

Microindentation for In Vivo Measurement of Bone Tissue Mechanical Properties in Humans. J. Bone Miner. Res. 25, 1877–1885. https://doi.org/10.1002/jbmr.73

Donnelly, E., Williams, R.M., Downs, S.A., Dickinson, M.E., Baker, S.P., van der Meulen, M.C., 2006. Quasistatic and dynamic nanomechanical properties of cancellous bone tissue relate to collagen content and organization. Journal of Materials Research 21, 2106–2117.

Faibish, D., Gomes, A., Boivin, G., Binderman, I., Boskey, A., 2005. Infrared imaging of calcified tissue in bone biopsies from adults with osteomalacia. Bone 36, 6–12. https://doi.org/10.1016/j.bone.2004.08.019

Fan, Z., Rho, J.-Y., 2003. Effects of viscoelasticity and time-dependent plasticity on nanoindentation measurements of human cortical bone. J Biomed Mater Res A 67, 208–214. https://doi.org/10.1002/jbm.a.10027

Farlay, D., Bala, Y., Rizzo, S., Bare, S., Lappe, J.M., Recker, R., Boivin, G., 2019. Bone remodeling and bone matrix quality before and after menopause in healthy women. Bone 128, 115030.

Farlay, D., Boivin, G., 2012. Bone Mineral Quality, in: Dionyssiotis, Y. (Ed.), Osteoporosis. InTech, p. ISBN 9780849391170; DOI: 10.5772/29091. https://doi.org/10.5772/29091

Farlay, D., Duclos, M.-E., Gineyts, E., Bertholon, C., Viguet-Carrin, S., Nallala, J., Sockalingum, G.D., Bertrand, D., Roger, T., Hartmann, D.J., Chapurlat, R., Boivin, G., 2011. The ratio 1660/1690 cm(-1) measured by infrared microspectroscopy is not specific of enzymatic collagen cross-links in bone tissue. PLoS ONE 6, e28736. https://doi.org/10.1371/journal.pone.0028736

Farlay, D., Panczer, G., Rey, C., Delmas, P.D., Boivin, G., 2010. Mineral maturity and crystallinity index are distinct characteristics of bone mineral. J. Bone Miner. Metab. 28, 433–445. https://doi.org/10.1007/s00774-009-0146-7

Follet, H., Boivin, G., Rumelhart, C., Meunier, P.J., 2004. The degree of mineralization is a determinant of bone strength: a study on human calcanei. Bone 34, 783–789.

Hadjidakis, D.J., Androulakis, I.I., n.d. Bone Remodeling. Annals of the New York Academy of Sciences 1092, 385–396. https://doi.org/10.1196/annals.1365.035

He, L.-H., Swain, M.V., 2009. Nanoindentation creep behavior of human enamel. Journal of Biomedical Materials Research Part A, An Official Journal of The Society for Biomaterials, The Japanese Society for Biomaterials, and The Australian Society for Biomaterials and the Korean Society for Biomaterials 91, 352–359.

Isaksson, H., Malkiewicz, M., Nowak, R., Helminen, H.J., Jurvelin, J.S., 2010a. Rabbit cortical bone tissue increases its elastic stiffness but becomes less viscoelastic with age. Bone 47, 1030–1038.

Isaksson, H., Nagao, S., Ma\Lkiewicz, M., Julkunen, P., Nowak, R., Jurvelin, J.S., 2010b. Precision of nanoindentation protocols for measurement of viscoelasticity in cortical and trabecular bone. Journal of biomechanics 43, 2410–2417.

Lefèvre, E., Farlay, D., Bala, Y., Subtil, F., Wolfram, U., Rizzo, S., Baron, C., Zysset, P., Pithioux, M., Follet, H., 2019. Compositional and mechanical properties of growing cortical bone tissue: a study of the human fibula. Scientific reports 9, 1–16.

Mirzaali, M.J., Schwiedrzik, J.J., Thaiwichai, S., Best, J.P., Michler, J., Zysset, P.K., Wolfram, U., 2016. Mechanical properties of cortical bone and their relationships with age, gender, composition and microindentation properties in the elderly. Bone 93, 196–211. https://doi.org/10.1016/j.bone.2015.11.018

Oliver, W.C., Pharr, G.M., 1992. An improved technique for determining hardness and elastic modulus using load and displacement sensing indentation experiments. Journal of materials research 7, 1564–1583.

Oyen, M.L., 2019. Handbook of Nanoindentation: With Biological Applications. CRC Press.

Oyen, M.L., 2008. Poroelastic nanoindentation responses of hydrated bone. Journal of Materials Research 23, 1307–1314.

Oyen, M.L., 2006. Nanoindentation hardness of mineralized tissues. Journal of biomechanics 39, 2699–2702.

Oyen, M.L., 2005. Spherical indentation creep following ramp loading. Journal of Materials Research 20, 2094–2100.

Oyen, M.L., Cook, R.F., 2003. Load–displacement behavior during sharp indentation of viscous–elastic–plastic materials. Journal of Materials Research 18, 139–150.

Oyen, M.L., Ko, C.-C., 2007. Examination of local variations in viscous, elastic, and plastic indentation responses in healing bone. Journal of Materials Science: Materials in Medicine 18, 623–628.

Paschalis, E.P., Verdelis, K., Doty, S.B., Boskey, A.L., Mendelsohn, R., Yamauchi, M., 2001. Spectroscopic characterization of collagen cross-links in bone. J. Bone Miner. Res. 16, 1821–1828. https://doi.org/10.1359/jbmr.2001.16.10.1821

Rho, J.Y., Kuhn-Spearing, L., Zioupos, P., 1998. Mechanical properties and the hierarchical structure of bone. Med Eng Phys 20, 92–102. https://doi.org/10.1016/s1350-4533(98)00007-1

Rho, J.Y., Pharr, G.M., 1999. Effects of drying on the mechanical properties of bovine femur measured by nanoindentation. J Mater Sci Mater Med 10, 485–488.

Rho, J.Y., Roy, M.E., Tsui, T.Y., Pharr, G.M., 1999. Elastic properties of microstructural components of human bone tissue as measured by nanoindentation. J. Biomed. Mater. Res. 45, 48–54. https://doi.org/10.1002/(sici)1097-4636(199904)45:1<48::aid-jbm7>3.0.co;2-5

Sakai, M., 1999. The Meyer hardness: A measure for plasticity? Journal of Materials Research 14, 3630–3639.

Tai, K., Qi, H.J., Ortiz, C., 2005. Effect of mineral content on the nanoindentation properties and nanoscale deformation mechanisms of bovine tibial cortical bone. Journal of Materials Science: Materials in Medicine 16, 947–959.

Tang, B., Ngan, A.H.W., Lu, W.W., 2007. An improved method for the measurement of mechanical properties of bone by nanoindentation. Journal of Materials Science: Materials in Medicine 18, 1875–1881.

Turner, C.H., Owan, I., Brizendine, E.J., Zhang, W., Wilson, M.E., Dunipace, A.J., 1996. High fluoride intakes cause osteomalacia and diminished bone strength in rats with renal deficiency. Bone 19, 595–601. https://doi.org/10.1016/s8756-3282(96)00278-5

Vandamme, M., Ulm, F.-J., 2006. Viscoelastic solutions for conical indentation. International Journal of solids and structures 43, 3142–3165.

Viguet-Carrin, S., Garnero, P., Delmas, P.D., 2006. The role of collagen in bone strength. Osteoporos Int 17, 319–336. https://doi.org/10.1007/s00198-005-2035-9

Wu, Z., Ovaert, T.C., Niebur, G.L., 2012. Viscoelastic properties of human cortical bone tissue depend on gender and elastic modulus. Journal of Orthopaedic Research 30, 693–699.

Zysset, P.K., Guo, X.E., Hoffler, C.E., Moore, K.E., Goldstein, S.A., 1999. Elastic modulus and hardness of cortical and trabecular bone lamellae measured by nanoindentation in the human femur. J Biomech 32, 1005–1012.

Figure List

Figure 1. Different steps of identifying the type of bone tissue for each indent using the reflection and the transmission electron microscopy. A) Identification of indents with the image obtained by reflection microscopy, B) Accurate positioning of indents and their types using a color code:-Triangle: "CSM" procedure,-Round: "Creep" procedure,-Orange: Osteoid tissue,-Green: Mineralized tissue,-Blue: Resin, C) Image obtained by transmission electron microscopy

Figure 2. A) Load-time (left) and load-displacement (right) curves obtained by instrumented indentation with CSM procedure, **B)** Load-time curves (right) and load-displacement (left) obtained by instrumented indentation with Creep procedure. **C)** Equations of Burgers Rheological model applied on loading and holding segments where: E_1, E_2 correspond to elastic modules and η_1, η_2 to viscosities. $\mathbf{E_1 = E_0, E_2 = G_V * 2 * (1 + \nu_0)}$. In the case of bone tissue, $\eta_1 >> \eta_2$. (with *resp* $\eta_1 = \eta_M$ and $\eta_2 = \eta_V$ from (Vandamme and Ulm, 2006)).

Figure 3. A) Relationship between collagen maturity and Mineral/Matrix ratio in both osteoid and mineralized tissue. **B)** Representative indentation in CSM mode into the two types of tissues (mineralized, Osteoid) and for Methyl methacrylate PMMA, **C)** Correlations between contact hardness (Hc), true hardness (H) and elastic modulus (E). Those plots show the strong linear dependence of Hc with elastic properties whereas H, reflecting plastic deformation is moderately linked to E.

Figure 4 A) Representative creep curve, **B)** Example of a displacement-time curves obtained during instrumented indentation method with the "creep" mode for six indents from the same sample, located in global tissue. An indicator of the maturity of collagen is placed to see the variation of this parameter according to the creep length.

Figure 5 Correlations obtained between parameters measured by FTIRM (left) Mineral/Matrix ratio, (Right) Collagen maturity and the micromechanical properties: **A)** E, **B)** H, and **C)** Hc, for the global bone tissue measurement and with separation of mineralized and osteoid phases. Mineral: dark black circle, Osteoid: open orange circle. Values for the measured parameter in the resin (PMMA) are in square green. Corresponding Rho Spearman correlation coefficient are indicated for each group.

Table List

Table 1. Descriptive statistics+ p-value for Mann-Whitney differences between mineral and osteoid phases

Table 2. Spearman coefficient of correlation between CSM, Burgers model mechanical properties and physicochemical properties. (-): NS: Non significant, *: $p<0.05$, **: $p<0.01$, ***: $p<0.001$

Table 1

	Parameters	unit	Tissue Type	n	Mean ±SD	Median	Min	Max	p-value
FTIRM	Mineral/Matrix		Global	156	2.15±1.96	1.86	0.065	5.83	
			Osteoid	67	0.20±0.18	0.13	0.065	0.78	<0.0001
			Mineral	93	3.62±1.28	3.93	0.18	5.83	
	Crystallinity	cm							
			Osteoid		N/A				
			Mineral	86	0.040±0.003	0.040	0.030	0.048	N/A
	Collagen maturity		Global	141	3.90±1.47	3.96	1.04	7.79	
			Osteoid	55	3.39±1.34	3.49	1.31	6.39	<0.0001
			Mineral	86	4.23±1.46	4.19	1.04	7.79	
CSM	E	GPa	Global	259	9.03±4.11	8.12	3.36	16.84	
			Osteoid	115	5.04±0.77	4.90	3.36	7.58	<0.0001
			Mineral	144	12.22±2.66	12.92	5.01	16.84	
			PMMA	20	3.59±0.46	3.70	2.72	4.20	
	Hc	GPa	Global	259	0.39±0.18	0.38	0.11	0.76	
			Osteoid	115	0.22±0.05	0.22	0.11	0.39	<0.0001
			Mineral	144	0.52±0.12	0.53	0.23	0.76	
			PMMA	20	0.15±0.03	0.16	0.09	0.20	
	H	GPa	Global	259	1.39±0.67	1.27	0.28	3.02	
			Osteoid	115	0.81±0.28	0.77	0.28	1.99	<0.0001
			Mineral	144	1.85±0.51	1.89	0.62	3.02	
			PMMA	20	0.49±0.16	0.54	0.25	0.73	
	W_{plast}/W_{tot}		Global	259	0.70±0.03	0.70	0.61	0.77	
			Osteoid	115	0.67±0.03	0.67	0.61	0.74	<0.0001
			Mineral	144	0.71±0.03	0.72	0.61	0.77	
			PMMA	20	0.68±0.02	0.68	0.66	0.72	
CREEP	E_1	GPa	Global	41	31.62±19.71	27.42	7.18	78.65	
			Osteoid	18	17.70±10.05	14.39	10.62	51.34	0.0002
			Mineral	23	42.52±10.05	38.18	14.9	78.65	
	E_2	GPa	Global	43	5.65±2.15	6.34	2.58	9.08	
			Osteoid	19	3.50±0.39	3.42	2.58	4.41	<0.0001
			Mineral	24	7.35±1.19	7.44	4.26	9.08	
	η_1	GPa.s	Global	43	2491±1326	2647	955	4763	
			Osteoid	19	1213±259	1097	955	1933	<0.0001
			Mineral	24	3504±861	3521	1517	4763	
	η_2	GPa.s	Global	43	4.86±1.85	4.31	1.49	9.76	
			Osteoid	19	3.23±0.71	3.49	1.49	4.28	<0.0001
			Mineral	24	6.15±1.39	5.94	3.70	9.76	
	L	µm	Global	43	0.61±0.20	0.55	0.36	0.94	
			Osteoid	19	0.81±0.11	0.84	0.60	0.94	<0.0001
			Mineral	24	0.46±0.08	0.44	0.36	0.70	

Table 2

			Mineral/Matrix	Crystallinity	Collagen maturity	E	Hc	H	W_{Plast}/W_{tot}	E_1	E_2	η_1	η_2
IRM	Crystallinity	Mineral	0.316**										
	Collagen maturity	Global	0.395***										
		Osteoid	-0.284*	N/A									
		Mineral	0.560***	0.238*									
CSM	E	Global	0.867***		0.272**								
		Osteoid	0.285*	N/A	-0.08NS								
		Mineral	0.647***	0.269*	0.410**								
	Hc	Global	0.831***		0.220*	0.946***							
		Osteoid	0.163 NS	N/A	-0.07 NS	0.730***							
		Mineral	0.558***	0.250 NS	0.269*	0.848***							
	H	Global	0.761***		0.183 NS	0.856***	0.970***						
		Osteoid	0.04 NS	N/A	-0.04 NS	0.451***	0.914***						
		Mineral	0.458***	0.207 NS	0.166 NS	0.610***	0.924***						
	W_{Plast}/W_{tot}	Global	0.575***	-0.01NS	0.106NS	0.681***	0.481***	0.322***					
		Osteoid	0.15NS	N/A	-0.06NS	0.233*	-0.383***	-0.693***					
		Mineral	0.111NS	-0.01NS	0.08NS	0.415***	0.02NS	-0.252**					
CREEP	E_1	Global	0.718***		0.401*	0.943**	1*	1*	0.600 NS				
		Osteoid	0.474*	N/A	-0.286 NS								
		Mineral	0.133 NS	0.304 NS	0.068 NS								
	E_2	Global	0.797***		0.539***	0.971***	0.971***	0.971***	0.618 NS	0.648***			
		Osteoid	0.339 NS	N/A	0.132 NS					-0.255 NS			
		Mineral	0.172 NS	0.157 NS	0.116 NS					0.322 NS			
	η_1	Global	0.828***		0.554***	0.829*	0.943**	0.943**	0.714 NS	0.807**	0.896***		
		Osteoid	0.261 NS	N/A	0.42 NS					0.136 NS	0.616***		
		Mineral	0.406*	0.388 NS	0.018 NS					0.756**	0.61***		
	η_2	Global	0.714***		0.465***	0.878*	0.878*	0.878*	0.878*	0.515**	0.909***	0.777***	
		Osteoid	-0.08 NS	N/A	-0.06 NS					-0.625**	0.504*	0.694NS	
		Mineral	0.003 NS	0.170 NS	0.025 NS					-0.015NS	0.769***	0.24NS	
	L	Global	-0.831***		-0.605***	-0.899*	-0.812*	-0.812*	-0.67NS	-0.700***	-0.890***	-0.971***	-0.890*
		Osteoid	-0.25 NS	N/A	-0.47[BL]					-0.122NS	-0.660***	-0.886***	0.132NS
		Mineral	-0.445*	-0.222NS	-0.134 NS					-0.685***	-0.565***	-0.910***	-0.06NS

* : p<0.05, ** : p<0.01 ; *** : p<0.001, BL : Borderline 0.05<p<0.06, NS : non significant

Figure 1

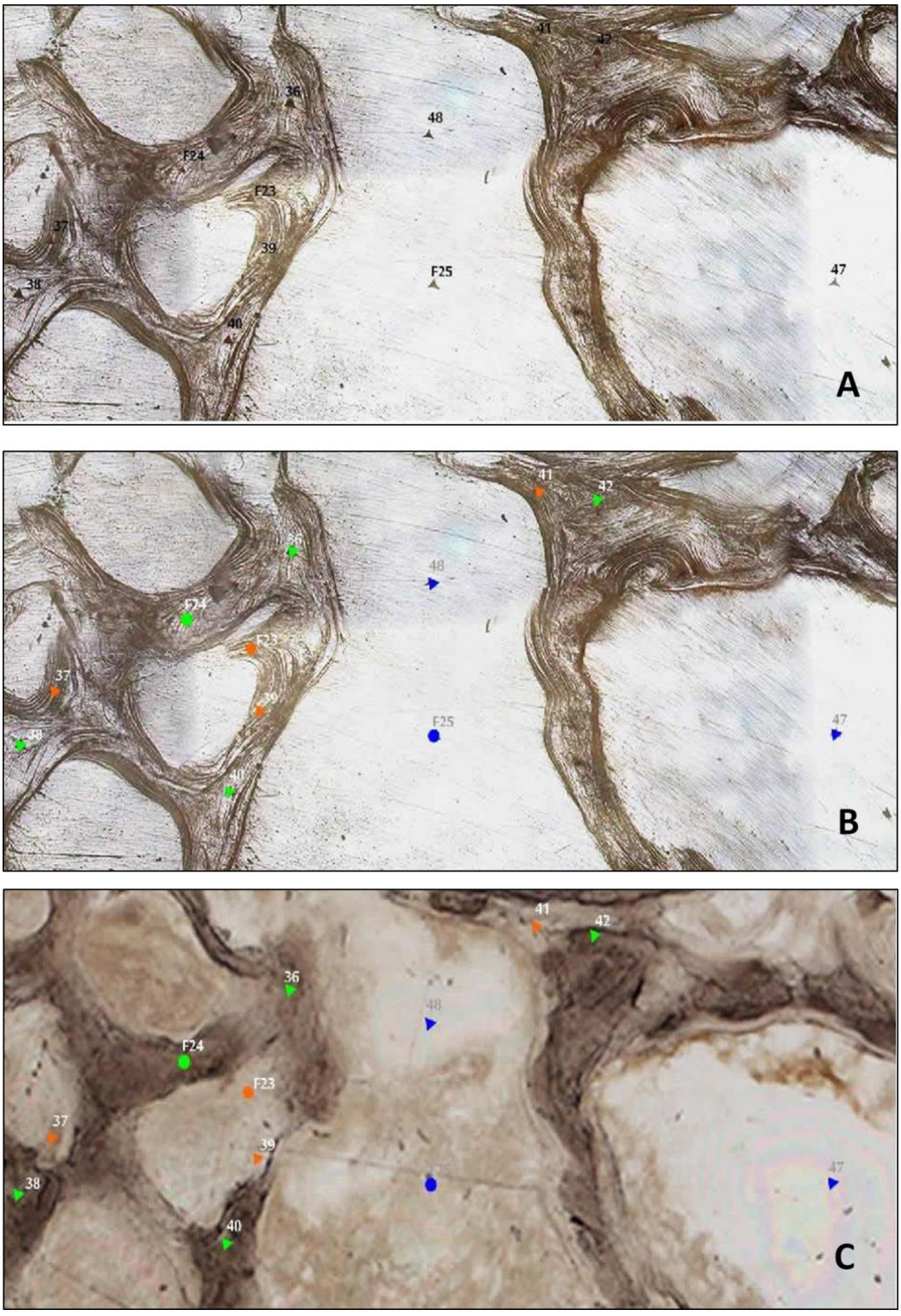
41
42
36
48
F24
F23
37
39
38
F25
47
40
A
41
42
36
48
F24
F23
37
39
38
F25
47
40
B
41
42
36
48
F24
F23
37
39
38
47
40
C

Figure 2

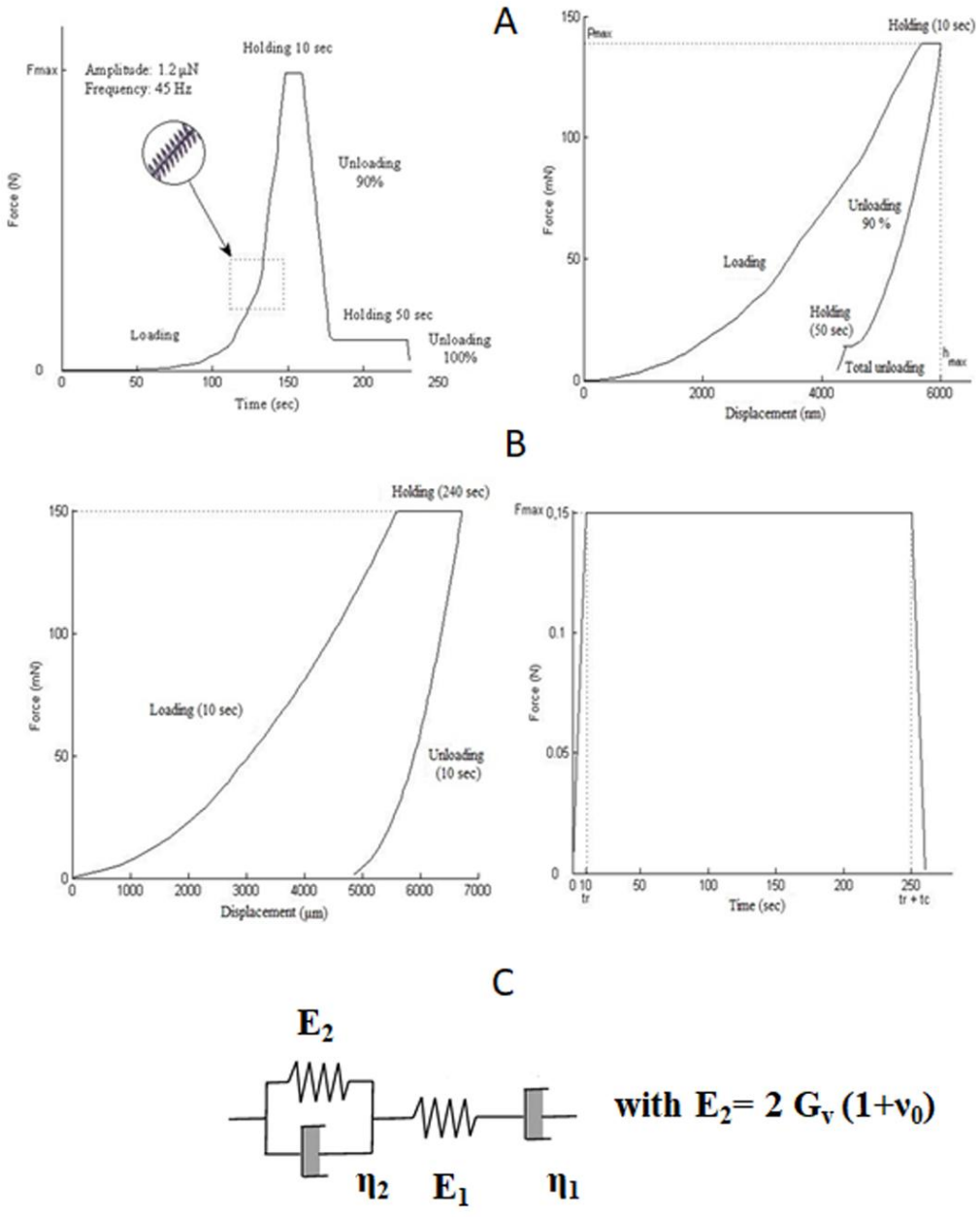
A
Fmax
Amplitude: 1.2 µN
Frequency: 45 Hz
Holding 10 sec
Unloading
90%
Holding 50 sec
Loading
Unloading
100%
Force (N)
Time (sec)
Pmax
Holding (10 sec)
Unloading
90 %
Loading
Holding
(50 sec)
Total unloading
h max
Force (mN)
Displacement (nm)
B
Holding (240 sec)
Loading (10 sec)
Unloading
(10 sec)
Force (mN)
Displacement (µm)
Fmax
Force (N)
tr
tr + tc
Time (sec)
C
E2
η2
E1
η1
with E2= 2 Gv (1+ν0)

Figure 3.

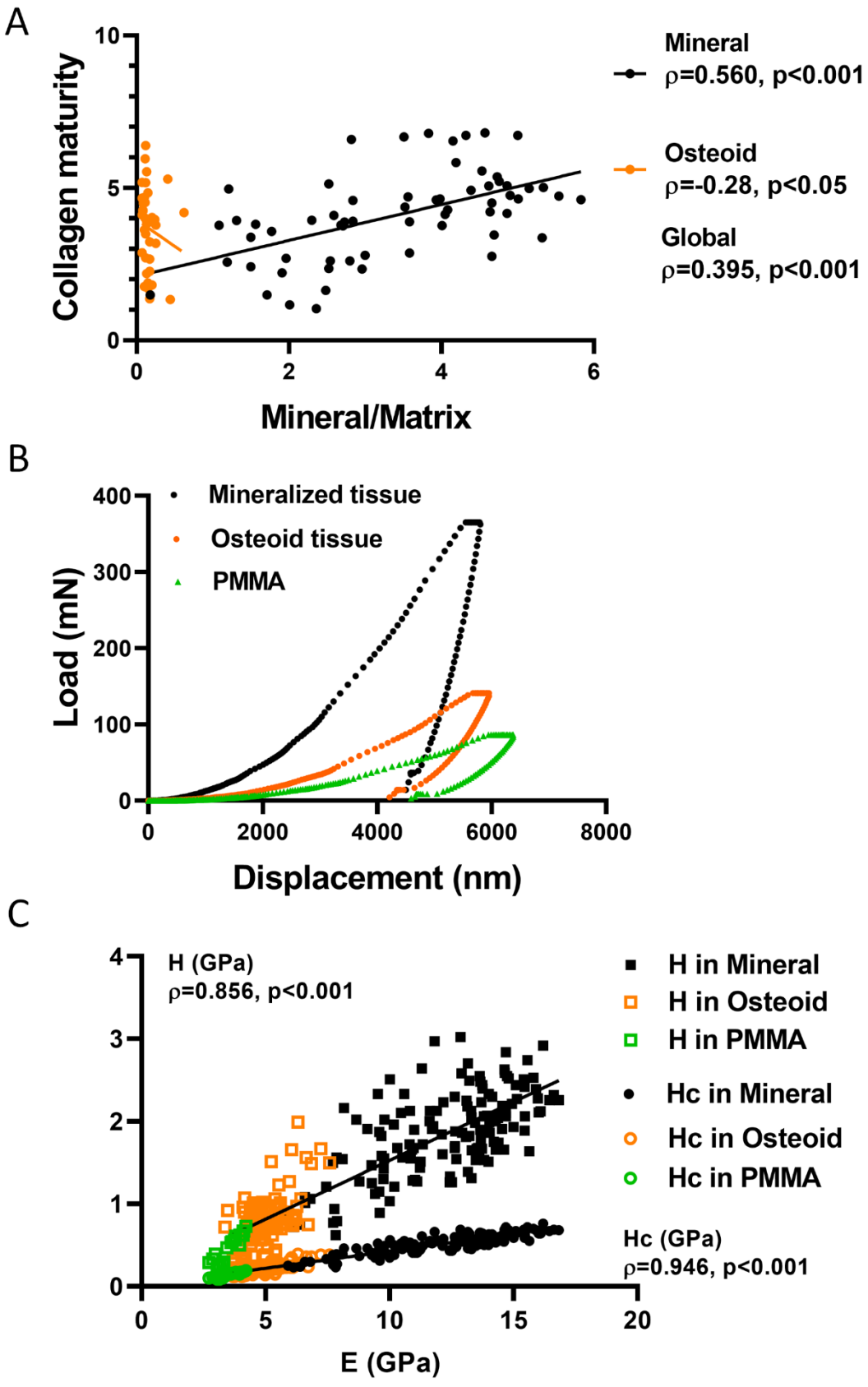
A
Collagen maturity
Mineral/Matrix
Mineral
ρ=0.560, p<0.001
Osteoid
ρ=-0.28, p<0.05
Global
ρ=0.395, p<0.001
B
Load (mN)
Displacement (nm)
Mineralized tissue
Osteoid tissue
PMMA
C
H (GPa)
ρ=0.856, p<0.001
E (GPa)
H in Mineral
H in Osteoid
H in PMMA
Hc in Mineral
Hc in Osteoid
Hc in PMMA
Hc (GPa)
ρ=0.946, p<0.001

Figure 4

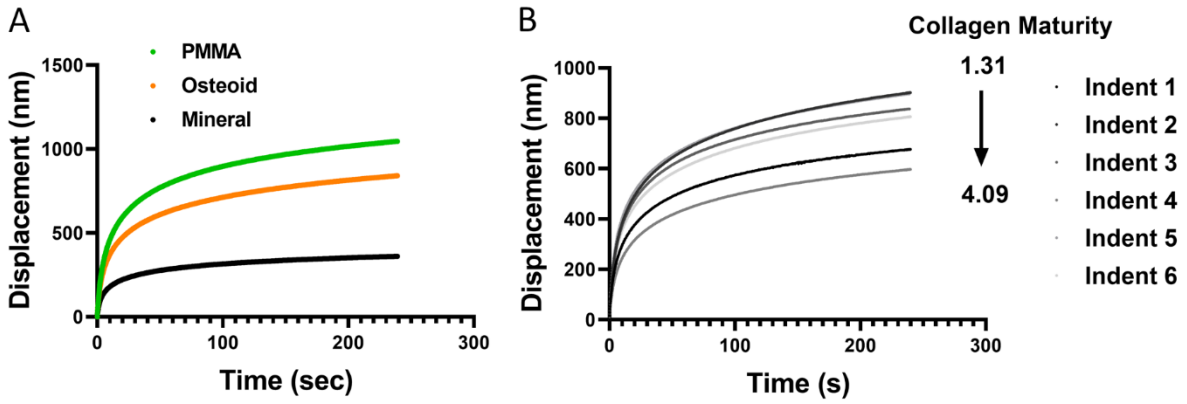
A
PMMA
Osteoid
Mineral
Displacement (nm)
1500
1000
500
0
0
100
200
300
Time (sec)
B
Collagen Maturity
1.31
4.09
Indent 1
Indent 2
Indent 3
Indent 4
Indent 5
Indent 6
Displacement (nm)
1000
800
600
400
200
0
0
100
200
300
Time (s)

Figure 5

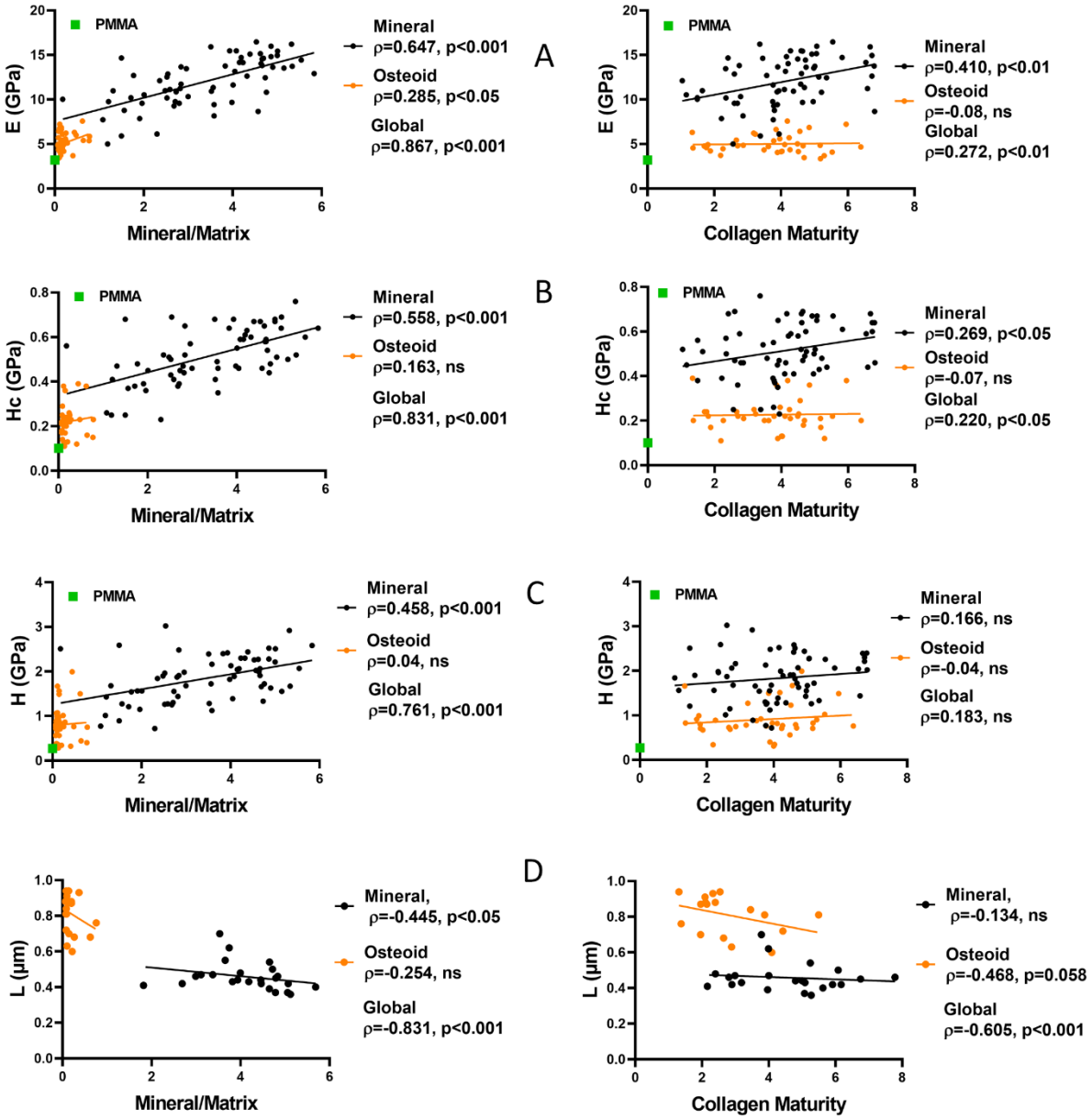
A
PMMA
E (GPa)
Mineral/Matrix
Mineral
ρ=0.647, p<0.001
Osteoid
ρ=0.285, p<0.05
Global
ρ=0.867, p<0.001
PMMA
E (GPa)
Collagen Maturity
Mineral
ρ=0.410, p<0.01
Osteoid
ρ=-0.08, ns
Global
ρ=0.272, p<0.01
B
PMMA
Hc (GPa)
Mineral/Matrix
Mineral
ρ=0.558, p<0.001
Osteoid
ρ=0.163, ns
Global
ρ=0.831, p<0.001
PMMA
Hc (GPa)
Collagen Maturity
Mineral
ρ=0.269, p<0.05
Osteoid
ρ=-0.07, ns
Global
ρ=0.220, p<0.05
C
PMMA
H (GPa)
Mineral/Matrix
Mineral
ρ=0.458, p<0.001
Osteoid
ρ=0.04, ns
Global
ρ=0.761, p<0.001
PMMA
H (GPa)
Collagen Maturity
Mineral
ρ=0.166, ns
Osteoid
ρ=-0.04, ns
Global
ρ=0.183, ns
D
L (µm)
Mineral/Matrix
Mineral,
ρ=-0.445, p<0.05
Osteoid
ρ=-0.254, ns
Global
ρ=-0.831, p<0.001
L (µm)
Collagen Maturity
Mineral,
ρ=-0.134, ns
Osteoid
ρ=-0.468, p=0.058
Global
ρ=-0.605, p<0.001